IEEE Access
Multidisciplinary | Rapid Review | Open Access Journal

Received December 20, 2020, accepted January 22, 2021, date of publication February 10, 2021, date of current version March 3, 2021.

Digital Object Identifier 10.1109/ACCESS.2021.3058384

Dynamic State Estimation Enabled Health Indicator for Parametric Fault Detection in Switching Power Converters

KANG YUE[1,2,3,4], (Student Member, IEEE), YU LIU[1], (Member, IEEE), PENG ZHAO[1], (Graduate Student Member, IEEE), BINGLIN WANG[1], (Student Member, IEEE), MINFAN FU[1], (Senior Member, IEEE), AND HAOYU WANG[1], (Senior Member, IEEE)

[1]School of Information Science and Technology, ShanghaiTech University, Shanghai 201210, China
[2]Shanghai Advanced Research Institute, Chinese Academy of Sciences, Shanghai 200050, China
[3]Shanghai Institute of Microsystem and Information Technology, Chinese Academy of Sciences, Shanghai 200050, China
[4]University of Chinese Academy of Sciences, Beijing 100049, China

Corresponding author: Yu Liu (liuyu.shanghaitech@gmail.com)

This work was supported in part by the National Natural Science Foundation of China under Grant 51807119 and in part by the Shanghai Pujiang Program under Grant 18PJ1408100.

ABSTRACT This article proposes a parametric fault detection method for switching power converters. The method generates a health indicator to represent the health condition of the entire power converter, and parametric faults are detected with any abnormality of the health indicator. The method first introduces a systematic mathematical modeling framework to describe all the physical laws of the switching power converter during healthy conditions. Afterwards, the dynamic state estimation via batch mode regression is applied to solve the states of the system and to generate the health indicator. The health indicator sensitively reflects the consistency between the actual measurement and the healthy circuit model by taking the statistic characteristics of solution into consideration. The proposed method only requires terminal measurements of the switching power converter, and does not have further assumptions on the topology of the converter. Compared to the existing observer based approaches, the method presents higher sensitivity during parametric faults. Compared to the existing parameter identification based approaches, the method does not need to estimate all the parameters of the converter in order to detect parametric faults. Simulation and experimental results on an example buck converter prove the validity of the proposed parametric fault detection method.

INDEX TERMS Parametric fault detection, switching power converters, dynamic states estimation, health indicator.

I. INTRODUCTION

Nowadays, with the growing penetration of switching power converters in smart grids, electric vehicles, data centers, motor drives and aerospace applications, safety and reliability of switching power converters are of increasing importance. ''Hard'' faults in switching power converters, such as semiconductors failure, capacitors failure, short-circuit/open-circuit faults, could cause sudden and catastrophic effect in the converters. Besides, ''Soft'' faults such as parametric faults (parameter drifts of key components) should also be carefully considered, since ''soft'' faults are usually related to degradation/aging and may evolve into ''hard'' faults. Fault detection is an effective way to detect the fault and ensure the safe and reliable operations of switching power converters by monitoring the system operating conditions through available measurements [1], [2]. The existing fault detection methods can be mainly classified into signal based methods, knowledge based methods, and model based methods [3], [4].

Signal based methods utilize the characteristics of measurement signals instead of mathematical models of the

The associate editor coordinating the review of this manuscript and approving it for publication was Lin Zhang.

circuit of interest for fault detection. These methods usually assume that specific signal characteristics will only emerge during faults. The fault detection decision is made based on clear extraction of the signal characteristics and prior information on the characteristics during faults. Examples of the extracted signal characteristics include time domain characteristics (magnitude of phase currents [5], magnetic component voltages [6], etc.) and frequency domain characteristics (spectrum of certain voltages or currents [7], [8], etc.). Mathematical tools such as fast Fourier transform, wavelet transform and spectral estimation can also be adopted to accurately extract the characteristics [9]–[11]. The main limitation of the signal based method is that it is generally hard to empirically select a certain set of characteristics that can clearly differentiate the fault conditions from the healthy conditions, especially for circuits with variable operation modes [12].

To avoid empirically selecting the fault characteristics from measurement signals, researchers proposed knowledge based methods (also known as data-driven methods). These methods treat the switching power converter of interest as a ''black box'' and can systematically extract the implicit fault characteristics by learning from a large number of historical data [13]. The knowledge based methods can be further categorized into qualitative methods (fault tree, expert system, etc.) [4] and quantitative methods (machine learning, support vector machine, neural networks, fuzzy logic, etc.) [14]–[18]. Nevertheless, these methods usually require a huge number of high-quality historical data for training. The data should cover a large number of fault scenarios and operating conditions, which may not be available in practice. Also, the computational cost of the training process is relatively high in general.

To make full use of both the available measurements and the converter circuit information (physical laws that the circuit should obey, including the characteristics of each converter circuit element, topology of the converter, etc.), researchers also proposed model based fault detection methods, which can be further classified into the following two groups. The first group of methods describes specific physical laws of the healthy switching power converter, and afterwards detects faults by examining whether the available measurements follow the specific physical laws. For example, to describe the overall health condition of the switching power converter, the observer based fault detection methods are widely adopted in literatures. The main idea of the observer based approaches is to construct an observer that is close to zero during normal operation and relatively large during faults, such as the difference between the actual and estimated measurements [19], [20], a user-defined function consisting of estimated states [21], etc. The first group of methods is usually adopted to detect ''hard'' faults, which correspond to complete failure (such as open circuit or short circuit) of a certain circuit element. Nevertheless, when dealing with parametric faults of the converter circuit (also known as ''soft'' faults), since these faults are not as severe as the ''hard'' faults, these methods may encounter sensitivity issues and therefore could sometimes fail to detect parametric faults. The second group of methods improves the performance of detecting parametric faults by directly identifying the corresponding parameter of a certain component of the converter. A parametric fault is detected if the difference between the estimated and the normal parameter value exceeds a certain threshold [22]. These methods further vary according to different ways of accurately identifying certain parameters. Reference [23] identifies the equivalent series resistance (ESR) and capacitance of the capacitor of interest by sampling the pulse width modulation signal and the capacitor output voltage in a buck converter. Reference [24] presents an adaptive parameter identification approach and utilizes the gradient descent algorithm to compute the parameters. Reference [25] identifies the parameters through Kalman Filter with the help of an additional injected signal with user-defined features. Reference [26] estimates the ESR of the capacitor by adding custom analog/digital circuits and calculating the ac losses of the capacitor. The limitations of the second group of methods are as follows. Firstly, in some literatures, additional hardware/injection of signals are required to identify the parameters of interest. Secondly and more importantly, if one wants to determine whether there are any parametric faults in the entire switching power converter, existing parameter identification based fault detection methods need to compute the parameters of all the circuit components, which may result in increased computational burden especially in complex switching power converters.

Considering the limitations of the existing methods, the aim of this article is to find ''one indicator'' that can sensitively demonstrate the overall system health condition: the ''one indicator'' should present obvious abnormality if there is any parametric fault inside the converter. Note that this article mainly focuses on the detection of ''soft'' faults (parameter drifts inside switching power converters such as inductors and capacitors). On one hand the desired algorithm should be able to sensitively detect even slight deviations of component parameters; on the other hand the algorithm could be designed in a slightly complex manner since the detection of ''soft'' faults does not require real-time computation (in comparison, the ''hard'' faults usually need to be detected as fast as possible with real-time computation, to avoid permanent damage to components inside switching power converters).

This article proposes a model based parametric fault detection method using the health indicator in switching power converters. The method first systematically builds the mathematical model of a general switching converter during healthy conditions, which describes all the physical laws that the switching power converter of interest should obey. The modeling procedure does not have additional assumptions on the topology of the switching power converter, and only requires terminal measurements of the converter. Next, with the help of dynamic state estimation (DSE) via batch mode regression, the method systematically solves the states of the

mathematical model and generates a general health indicator that reflects the health condition of the entire switching power converter. The health indicator sensitively demonstrates the consistency between the available measurements and the mathematical model of the healthy converter through full utilization of the statistic characteristics of the solution. Parametric faults are detected if the health indicator presents abnormality. The contributions of the article are summarized as follows,

- The proposed method fully considers the physical laws of a general switching power converter; no additional assumptions on the topology of the switching power converter are required;
- The proposed method only requires terminal measurements of the switching power converter; no additional sensors, analogy circuits, or injection of external signals are required;
- The proposed method extracts one health indicator for parametric fault detection in the entire switching power converter; compared to the existing observer based methods, the proposed method has improved sensitivity to reliably detect parametric faults; compared to the existing parameter identification based methods, it is not necessary to estimate all the parameters of the circuit at the same time in order to detect parametric faults.

The remainder of this article is organized as follows. Section II introduces the systematic modeling framework of a general switching power converter. Section III generates the health indicator for fault detection based on DSE. Section IV and V demonstrate the simulation and experimental results of parametric fault detection on an example buck converter, to verify the effectiveness of the proposed method. Section VI draws a conclusion.

II. SYSTEMATIC MODELING FRAMEWORK

The proposed model based parametric fault detection method requires an accurate mathematical model of the circuit. This section introduces a systematic framework to mathematically model a general switching power converter during healthy conditions. The mathematical model accurately describes all the physical laws that the switching power converter of interest should obey. Note that this modeling framework does not have any assumptions on the topology of the converter.

A. MATHEMATICAL MODEL IN DIFFERENTIAL AND ALGEBRAIC FORM

A general switching power converter usually consists of power sources, switches (diodes, MOSFETs, IGBTs, etc), linear elements (inductors, capacitors, resistors, transformers) and sometimes even nonlinear elements (transformers with saturation characteristics, nonlinear resistors, etc.). As a switched system, the power converter can be described via a hybrid nonlinear mathematical model in general. The hybrid nonlinear model consists of not only continuous variables $x_i(t)$ $(i = 1, 2, \ldots, n)$ such as the instantaneous voltage across or current through each branch, but also discrete (or binary 1/0) variables $S_j(t)$ $(j = 1, 2, \ldots, n_S)$ that represent the on/off status of each switch, where n is the number of states of the system and n_S is the number of switches. The hybrid nonlinear mathematical model in the differential and algebraic form has the following standard syntax,

$$\begin{aligned}
\boldsymbol{z}_{actual}(t) &= \boldsymbol{A}_{eq1,S(t)}\boldsymbol{x}(t) + \boldsymbol{B}_{eq1,S(t)}d\boldsymbol{x}(t)/dt + \boldsymbol{C}_{eq1,S(t)} \\
\boldsymbol{0} &= \boldsymbol{A}_{eq2,S(t)}\boldsymbol{x}(t) + \boldsymbol{B}_{eq2,S(t)}d\boldsymbol{x}(t)/dt + \boldsymbol{C}_{eq2,S(t)} \\
\boldsymbol{y}_{actual}(t) &= \boldsymbol{A}_{eq3,S(t)}\boldsymbol{x}(t) + \boldsymbol{C}_{eq3,S(t)} \\
\boldsymbol{0} &= \boldsymbol{A}_{eq4,S(t)}\boldsymbol{x}(t) + \begin{bmatrix} \cdots \\ \boldsymbol{x}(t)^T \cdot \boldsymbol{F}^{(i)}_{eq4,S(t)} \cdot \boldsymbol{x}(t) \\ \cdots \end{bmatrix} \\
&\quad + \boldsymbol{C}_{eq4,S(t)}
\end{aligned} \tag{1}$$

where $\boldsymbol{x}(t)$ and $\boldsymbol{S}(t)$ are the state vector and the switch status vector (with elements of $x_i(t)$ and $S_j(t)$ respectively);$\boldsymbol{z}_{actual}(t)$ and $\boldsymbol{y}_{actual}(t)$ are the actual measurement vectors at terminals of the circuit corresponding to the differential equations and algebraic equations, respectively; $\boldsymbol{A}_{eq1,S(t)}$, $\boldsymbol{B}_{eq1,S(t)}$, $\boldsymbol{C}_{eq1,S(t)}$, $\boldsymbol{A}_{eq2,S(t)}$, $\boldsymbol{B}_{eq2,S(t)}$, $\boldsymbol{C}_{eq2,S(t)}$, $\boldsymbol{A}_{eq3,S(t)}$, $\boldsymbol{C}_{eq3,S(t)}$, $\boldsymbol{A}_{eq4,S(t)}$, $\boldsymbol{F}^{(i)}_{eq4,S(t)}$, and $\boldsymbol{C}_{eq4,S(t)}$ are the corresponding coefficient matrices as functions of $\boldsymbol{S}(t)$. Note that the syntax in (1) is a set of algebraic and first-order differential equations with the maximum nonlinearities of 2. Additional state variables could be introduced to ensure the validity of this syntax if the physical laws of the switching power converter follow differential equations with higher order or higher nonlinearities. The physical meaning of each row in (1) is summarized in Table 1.

TABLE 1. Physical meaning of each row in (1).

Row	*Physical Meaning*
1	Physical laws between actual measurements and states, differential equations
2	Internal constraints among states, differential equations
3	Physical laws between actual measurements and states, algebraic equations
4	Internal constraints among states, algebraic equations (including nonlinearity)

Specifically, different combinations of switch on/off status correspond to different operating modes of the switching power converter. For each operating mode, the hybrid mathematical model in (1) can be transformed into (2), where $\boldsymbol{A}_{eq1}$, $\boldsymbol{B}_{eq1}$, $\boldsymbol{C}_{eq1}$, $\boldsymbol{A}_{eq2}$, $\boldsymbol{B}_{eq2}$, $\boldsymbol{C}_{eq2}$, $\boldsymbol{A}_{eq3}$, $\boldsymbol{C}_{eq3}$, $\boldsymbol{A}_{eq4}$, $\boldsymbol{F}^{(i)}_{eq4}$, and $\boldsymbol{C}_{eq4}$ are the corresponding coefficient matrices, other definitions are the same as those in (1). The detailed mathematical model in differential and algebraic form of an example buck converter is shown in the Appendix.

$$\begin{aligned}
\boldsymbol{z}_{actual}(t) &= \boldsymbol{A}_{eq1}\boldsymbol{x}(t) + \boldsymbol{B}_{eq1}d\boldsymbol{x}(t)/dt + \boldsymbol{C}_{eq1} \\
\boldsymbol{0} &= \boldsymbol{A}_{eq2}\boldsymbol{x}(t) + \boldsymbol{B}_{eq2}d\boldsymbol{x}(t)/dt + \boldsymbol{C}_{eq2} \\
\boldsymbol{y}_{actual}(t) &= \boldsymbol{A}_{eq3}\boldsymbol{x}(t) + \boldsymbol{C}_{eq3} \\
\boldsymbol{0} &= \boldsymbol{A}_{eq4}\boldsymbol{x}(t) + \begin{bmatrix} \cdots \\ \boldsymbol{x}(t)^T \cdot \boldsymbol{F}^{(i)}_{eq4} \cdot \boldsymbol{x}(t) \\ \cdots \end{bmatrix} + \boldsymbol{C}_{eq4}
\end{aligned} \tag{2}$$

B. MATHEMATICAL MODEL IN ALGEBRAIC FORM

In order to solve the states in the mathematical model, the model in the differential and algebraic form in (2) is discretized into the model in the pure algebraic form. Here the trapezoidal integration method is selected as an example. The first two sets of equations in (2) are integrated over time interval [t-h, t], where h is the sample interval. The mathematical model in the algebraic form can be written as,

$$\begin{aligned} \boldsymbol{z}(t) &= \boldsymbol{M}\boldsymbol{x}(t) + \boldsymbol{N}\boldsymbol{x}(t-h) - \boldsymbol{z}(t-h) + \boldsymbol{C}_1 \\ \boldsymbol{y}(t) &= \boldsymbol{G}\boldsymbol{x}(t) + \begin{bmatrix} \cdots \\ \boldsymbol{x}(t)^T \cdot \boldsymbol{F}^{(i)} \cdot \boldsymbol{x}(t) \\ \cdots \end{bmatrix} + \boldsymbol{C} \end{aligned} \tag{3}$$

where $\boldsymbol{z}(t) = [\,\boldsymbol{z}_{actual}(t)\ \boldsymbol{0}\,]^T$ and $\boldsymbol{y}(t) = [\,\boldsymbol{y}_{actual}(t)\ 0\,]^T$ are the extended measurement vectors (including $\boldsymbol{0}$ as the virtual measurements); $\boldsymbol{z}(t-h)$ and $\boldsymbol{x}(t-h)$ are the past history vectors of the extended measurement and states. The parameter matrices are, $\boldsymbol{M} = [\boldsymbol{A}_{eq1} + 2\boldsymbol{B}_{eq1}/h, \boldsymbol{A}_{eq2} + 2\boldsymbol{B}_{eq2}/h]^T$, $\boldsymbol{N} = [\boldsymbol{A}_{eq1} - 2\boldsymbol{B}_{eq1}/h,\ \boldsymbol{A}_{eq2} - 2\boldsymbol{B}_{eq2}/h]^T$, $\boldsymbol{C}_1 = [2\boldsymbol{C}_{eq1}, 2\boldsymbol{C}_{eq2}]^T$, $\boldsymbol{G} = [\boldsymbol{A}_{eq3}, \boldsymbol{A}_{eq4}]^T$, $\boldsymbol{F}^{(i)} = \boldsymbol{F}^{(i)}_{eq4}$ for the virtual measurement rows, and $\boldsymbol{C} = [\boldsymbol{C}_{eq3}, \boldsymbol{C}_{eq4}]^T$.

Afterwards, rewrite (3) in the discrete form,

$$\begin{aligned} \boldsymbol{x}_k &= \boldsymbol{A}\boldsymbol{x}_{k-1} + \boldsymbol{B}\boldsymbol{u}_k \\ \boldsymbol{y}_k &= h(\boldsymbol{x}_k) = \boldsymbol{G}\boldsymbol{x}_k + \begin{bmatrix} \cdots \\ \boldsymbol{x}_k^T \cdot \boldsymbol{F}^{(i)} \cdot \boldsymbol{x}_k \\ \cdots \end{bmatrix} + \boldsymbol{C} \end{aligned} \tag{4}$$

where, $\boldsymbol{A} = -\boldsymbol{M}^{-1}\boldsymbol{N}$; $\boldsymbol{B}$ is the identity matrix; $\boldsymbol{u}_k = \boldsymbol{M}^{-1}(\boldsymbol{z}_k + \boldsymbol{z}_{k-1} - \boldsymbol{C}_1)$; subscripts k and k-1 represent the values at time t and t-h, respectively.

III. HEALTH INDICATOR FOR PARAMETRIC FAULT DETECTION BASED ON DSE

This section introduces the procedure of extracting the health indicator for parametric fault detection in a general switching power converter. The key idea of the health indicator is to examine whether the available instantaneous measurements are consistent with all the physical laws that the switching power converters during healthy conditions should obey (described by the accurate mathematical model of the circuit). Therefore, the health indicator provides a systematic metric of the overall health condition of the entire switching power converter, and deviations of the parameters inside the converter (parametric faults) will be reflected by the health indicator.

A. DSE VIA BATCH MODE REGRESSION

To systematically solve the mathematical model of a general switching power converter in (4), the DSE via batch mode regression is utilized. The model and measurement error vectors $\boldsymbol{\omega}_k$ and $\boldsymbol{v}_k$ are the errors of the first and the second set of equations in (4), respectively. The errors are assumed to obey Gaussian distribution, which are good approximations for practical circuits: $\boldsymbol{\omega}_k \sim N(0, \boldsymbol{Q})$ and $\boldsymbol{v}_k \sim N(0, \boldsymbol{R})$.

The first step is to predict the estimated states $\hat{\boldsymbol{x}}_{k|k-1}$ using the first set of equations in (4),

$$\begin{aligned} \hat{\boldsymbol{x}}_{k|k-1} &= \boldsymbol{A}\hat{x}_{k-1} + \boldsymbol{B}\boldsymbol{u}_k \\ \boldsymbol{P}_{k|k-1} &= \boldsymbol{A}\boldsymbol{P}_{k-1}\boldsymbol{A}^T + \boldsymbol{Q} \end{aligned} \tag{5}$$

where $\boldsymbol{x}_k$ and $\hat{\boldsymbol{x}}_k$ are the actual and the estimated state vectors at step k, $\boldsymbol{P}_k$ (or $\boldsymbol{P}_{k|k-1}$) is the covariance matrix of the errors of the estimated state vector $\hat{\boldsymbol{x}}_k$ (or $\hat{\boldsymbol{x}}_{k|k-1}$).

The second step is to observe the fact that $\hat{\boldsymbol{x}}_{k|k-1}$ can be treated as a new set of "measurements" of $\boldsymbol{x}_k$ with error $\boldsymbol{e}_k \sim N(0, \boldsymbol{P}_{k|k-1})$. By adding the second set of equations in (4) as another set of measurements, the dynamic state estimation problem can be formulated using the batch mode regression. The best estimates of the state vector is equivalent to solving the following optimization problem,

$$\min_{\boldsymbol{x}_k} J = \boldsymbol{r}_k^T \boldsymbol{W} \boldsymbol{r}_k \tag{6}$$

where $\boldsymbol{r}_k$ is the residual vector, $\boldsymbol{W}$ is the weight matrix, $\boldsymbol{r}_k = \begin{bmatrix} \boldsymbol{y}_k \\ \hat{\boldsymbol{x}}_{k|k-1} \end{bmatrix} - \begin{bmatrix} h(\boldsymbol{x}_k) \\ \boldsymbol{x}_k \end{bmatrix}$ and $\boldsymbol{W} = \begin{bmatrix} \boldsymbol{R}_k^{-1} & \\ & \boldsymbol{P}_{k|k-1}^{-1} \end{bmatrix}$.

The best estimates of the state vector $\hat{\boldsymbol{x}}_k$ can be solved through the following iterative algorithm until convergence,

$$\begin{aligned} \hat{\boldsymbol{x}}_k^{\nu+1} = \hat{\boldsymbol{x}}_k^{\nu} &+ \left(\begin{bmatrix} \boldsymbol{H}^T & \boldsymbol{I} \end{bmatrix} \boldsymbol{W} \begin{bmatrix} \boldsymbol{H} \\ \boldsymbol{I} \end{bmatrix} \right)^{-1} \begin{bmatrix} \boldsymbol{H}^T & \boldsymbol{I} \end{bmatrix} \\ &\times \boldsymbol{W} \left(\begin{bmatrix} \boldsymbol{y}_k \\ \hat{\boldsymbol{x}}_{k|k-1} \end{bmatrix} - \begin{bmatrix} h(\hat{\boldsymbol{x}}_k^{\nu}) \\ \hat{\boldsymbol{x}}_k^{\nu} \end{bmatrix} \right) \end{aligned} \tag{7}$$

where $\boldsymbol{H}_k = \partial h/\partial \boldsymbol{x}|_{\boldsymbol{x}=\hat{\boldsymbol{x}}_k^{\nu}}$, and $\boldsymbol{I}$ is the identity matrix with the dimension of the number of states.

After simplification, equation (7) can be equivalently transformed into (8),

$$\hat{\boldsymbol{x}}_k^{\nu+1} = \hat{\boldsymbol{x}}_{k|k-1} + \boldsymbol{K}_k \left[\boldsymbol{y}_k - h\left(\hat{\boldsymbol{x}}_k^{\nu}\right) + \boldsymbol{H}_k \left(\hat{\boldsymbol{x}}_k^{\nu} - \hat{\boldsymbol{x}}_{k|k-1} \right) \right] \tag{8}$$

where $\boldsymbol{K}_k = (\boldsymbol{H}_k^T \boldsymbol{R}_k^{-1} \boldsymbol{H}_k + \boldsymbol{P}_{k|k-1}^{-1})^{-1} \boldsymbol{H}_k^T \boldsymbol{R}_k^{-1}$, $\boldsymbol{H}_k = \partial h/\partial \boldsymbol{x}|_{\boldsymbol{x}=\hat{\boldsymbol{x}}_k^{\nu}}$, and $\boldsymbol{P}_k$ can be approximated as $\boldsymbol{P}_k = (\boldsymbol{I} - \boldsymbol{K}_k \boldsymbol{H}_k)\boldsymbol{P}_{k|k-1}$.

Note that when the power electronic converter is switching between two different operating modes, the variables (including measurements, estimated states, etc.) at the end of this operating mode should be used as the initial conditions of the next operating mode to ensure continuous estimation of dynamic states of the power electronic converter.

B. STATISTICS BASED HEALTH INDICATOR

After calculating the best estimates of the state vector $\hat{\boldsymbol{x}}_k$, the consistency between the measurements and mathematical model of the switching power converter can be quantified by the chi-square value J after substituting $\boldsymbol{x}_k = \hat{\boldsymbol{x}}_k$ into (6). If the switching power converter is healthy, the actual measurements should match the model very well, with relatively small J; otherwise, if there is any parametric fault (or even failure of a specific element, such as open/short circuit), the actual measurements will deviate from the model, with relatively large J.

There are many ways to generate the health indicator from the chi-square value J. One common way is to use the max/min/average value of J: a fault is detected if the max/min/average value of J exceeds a certain threshold. Nevertheless, this may result in inadequate sensitivity since the parametric faults are relatively mild compared to the complete failure of a specific element. To solve this problem, we can make full use of the statistic characteristic of chi-square value J: if the errors $\boldsymbol{\omega}_k$ and $\boldsymbol{v}_k$ obey Gaussian distributions, the chi-square value should obey the χ^2 distribution: $J \sim \chi^2(m)$, where m is the degree of freedom, which is the difference between the numbers of measurements and states [27].

Therefore, a parametric fault can be detected if the actual distribution of the chi-square value J is very different from the ideal distribution of the value J. There are various schemes to compare the two distributions. Here we adopt one straightforward way as an example. First, choose a probability α_{set} ($0 < \alpha_{set} < 1$). With the degree of freedom m and the user-defined probability α_{set}, we can find the value ξ such that,

$$P(\xi, m) = \alpha_{set} \tag{9}$$

where $P(\xi, m)$ is the probability of the χ^2 distribution given $\chi^2 \leq \xi$ and m degree of freedom.

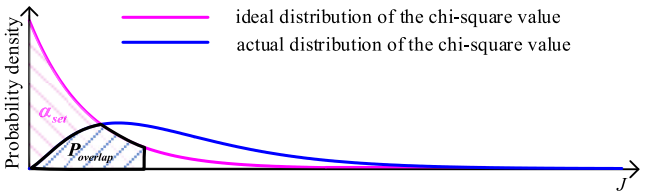

FIGURE 1. Health indicator based on distribution curve difference.

After depicting the distribution of the calculated chi-square value, the overlap area between the ideal and the actual distribution curves is defined as $P_{overlap}$, as shown in Fig. 1. If the switching power converter is healthy, the overlap area $P_{overlap}$ should be close to α_{set}; if there are parametric faults, $P_{overlap}$ will be much less than α_{set}. The health indicator (within the range from 0 to 1) is defined as,

$$HI = P_{overlap} / \alpha_{set} \tag{10}$$

One can observe that HI should be close to 1 during normal operation. Therefore, parametric faults are detected if

$$HI < HI_{set} \tag{11}$$

where, HI_{set} is the user-defined threshold (less than 1) that can be determined empirically.

To sum up, the flow chart of the proposed parametric fault detection procedure is shown in Fig. 2.

IV. SIMULATION RESULTS

This section verifies the performance of the proposed health indicator for parametric fault detection through simulation.

TABLE 2. Simulation and experiment setup of the system.

Variables	*Values*	*Variables*	*Values*
$v_{in}(t)$	24 V	C	55 μF
Duty Cycle	0.5	R_C	0.002 Ω
R	20 Ω	L	518 μH
Switching Frequency	20 kHz	R_L	0.64 Ω

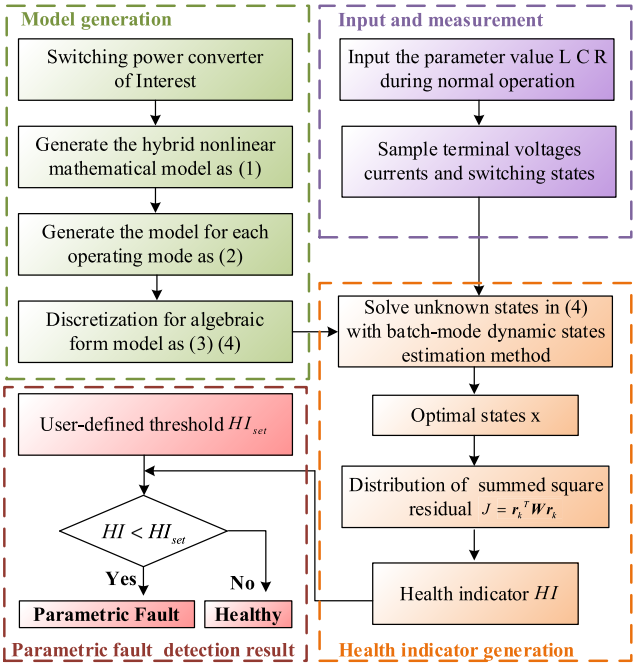

FIGURE 2. Flowchart of proposed parametric fault detection procedure.

The example switching power converter of interest is a dc-dc buck converter as shown in Fig. 23 of the Appendix. The setup of the system during normal conditions is shown in Table 2. The sampling rate of the system is 5MHz. The available measurements are also defined in the Appendix. Here Gaussian distributed measurement errors with 0.1 % standard deviations are added to the measurements. The initial value of $\boldsymbol{P}$ is selected as a relatively large number $\boldsymbol{P}_0 = 10^{10}\boldsymbol{I}$ per unit, where $\boldsymbol{I}$ is the identity matrix with the dimension of the number of states. In this case, the user-defined settings are selected as $\alpha_{set} = 0.5$ and $HI_{set} = 0.8$ empirically to ensure sensitivity and robustness of the parametric fault detection procedure. Here a 5 ms time window is adopted to depict the distribution of the calculated chi-square value. Next, the performance of the proposed method is validated via different operating conditions with different parametric faults.

A. NORMAL OPERATION

The measurements during normal operation are shown in Fig. 3. To demonstrate the results of DSE, here we select the actual measurements, estimated measurements and residuals (differences between the actual and the estimated measurements) of $i_{in}(t)$ as examples, as shown in Fig. 4. One can observe that the residuals are very close to zero.

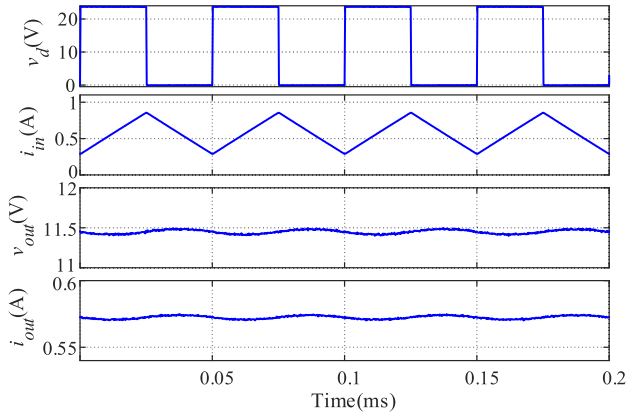

FIGURE 3. Measurements during normal operation, simulation results.

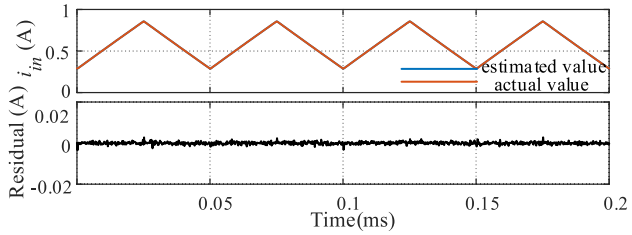

FIGURE 4. Residuals of $i_{in}(t)$ during normal operation, simulation results.

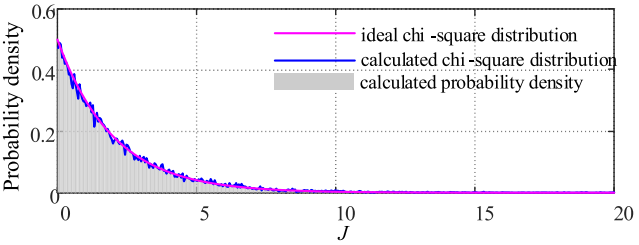

FIGURE 5. Distribution of calculated chi-square value during normal operation, simulation results.

The distribution of the calculated chi-square value is depicted in Fig. 5. It can be observed that the calculated distribution is very consistent with the ideal distribution. The calculated health indicator is $HI = 0.9498 > HI_{set}$. Therefore, the system is healthy and no parametric fault is detected.

B. PARAMETRIC FAULTS OF THE INDUCTOR ONLY

A group of parametric faults of the inductor is studied. The parametric faults are simulated by updating the inductance value L from the normal value (518 μH) to 489 μH, 460 μH, 440 μH, 382 μH and 298 μH, respectively. Other parameters of the power electronic circuit remain the same. The measurements during different inductor parametric faults are shown in Fig. 6. One can observe that the measurements change slightly due to the parametric faults. The actual measurements, estimated measurements and residuals of $i_{in}(t)$ with an example parametric fault of $L = 489$ μH are shown in Fig. 7. One can observe that the residuals become larger compared

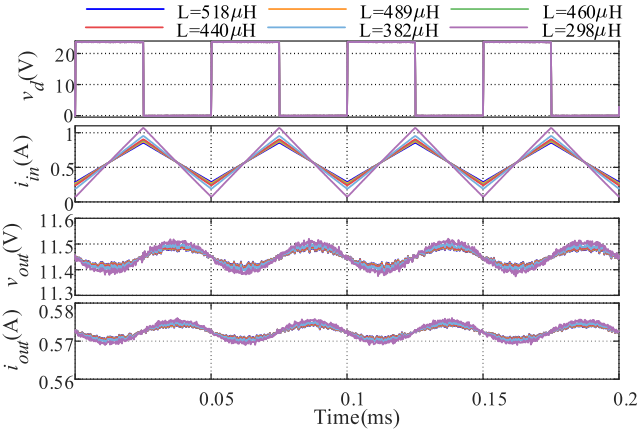

FIGURE 6. Measurements during parametric faults of the inductor, simulation results.

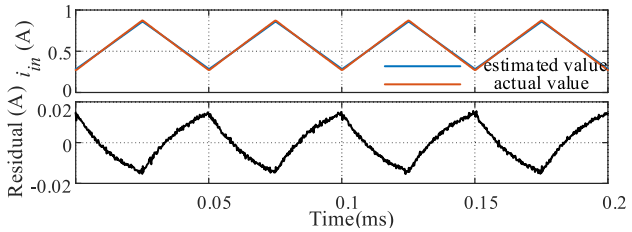

FIGURE 7. Residuals of $i_{in}(t)$ during parametric faults of the inductor: $L = 489\mu$H, simulation results.

to those during normal operation, indicating possible inconsistency between the measurements and the model.

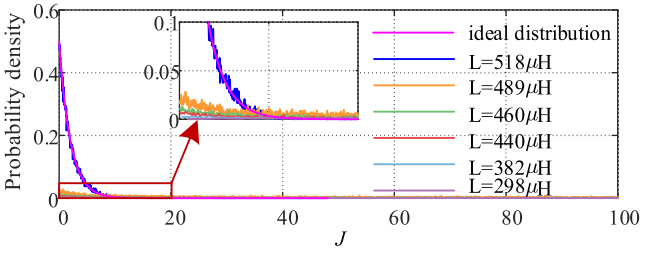

FIGURE 8. Distributions of calculated chi-square value during parametric faults of the inductor, simulation results.

To further quantify this inconsistency, the distributions of the calculated chi-square value during different inductor parametric faults are depicted in Fig. 8. It can be observed that the calculated distributions are quite different from the ideal distribution; and more severe inductor parametric fault corresponds to larger difference between the calculated distribution and the ideal distribution. The calculated health indicators with 489, 460, 440, 382 and 298 μH inductances are $HI = 0.0301$, 0, 0, 0, and 0, respectively. Therefore, since $HI < HI_{set}$ for all above scenarios, parametric faults inside the system are successfully detected.

C. PARAMETRIC FAULTS OF THE CAPACITOR ONLY

A group of parametric faults of the capacitor is studied. The parametric faults are simulated by updating the capacitance value C from the normal value (55 μF) to 40 μF, 28 μF,

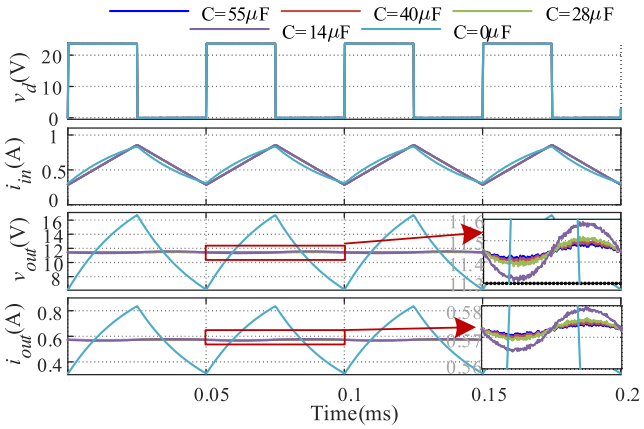

FIGURE 9. Measurements during parametric faults of the capacitor, simulation results.

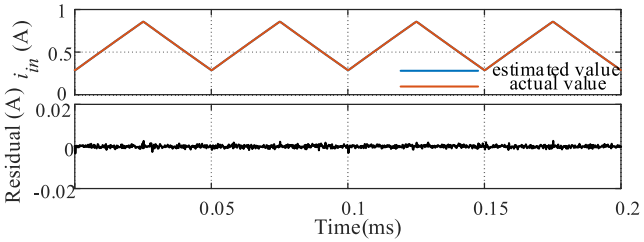

FIGURE 10. Residuals of $i_{in}(t)$ during parametric faults of the capacitor: $C = 40\mu$F, simulation results.

14 μF and 0 μF, respectively. Other parameters of the power electronic circuit remain the same. The measurements during different capacitor parametric faults are shown in Fig. 9. One can observe that, except for the complete failure of the capacitance (0 μF), the measurements change slightly due to the parametric faults. The actual measurements, estimated measurements and residuals of $i_{in}(t)$ with an example parametric fault of $C = 40$ μF are shown in Fig. 10. One can observe that the residuals are still quite small and do not increase significantly compared to those during normal operation, and therefore by only observing the magnitude of residuals one may not be able to reliably detect the capacitor parametric faults. This is consistent with the fact that capacitor parametric faults are more difficult to be detected than the inductor parametric faults.

The proposed method improves the parametric fault detection sensitivity by considering the statistic characteristics of the chi-square value. The distributions of the calculated chi-square value during different capacitor parametric faults are depicted in Fig. 11. It can be observed that the calculated distributions are quite different from the ideal distribution; and more severe capacitor parametric fault corresponds to larger difference between the calculated distribution and the ideal distribution. The calculated health indicators with 40, 28, 14 and 0 μF capacitances are $HI = 0.4251$, 0.1071, 0.0058, and 0, respectively. Therefore, since $HI < HI_{set}$ for all above scenarios, parametric faults inside the system are successfully detected.

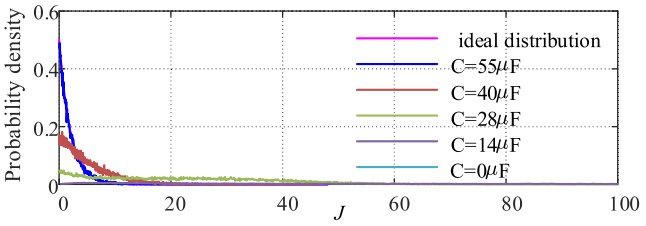

FIGURE 11. Distributions of calculated chi-square value during parametric faults of the capacitor, simulation results.

1) DEMONSTRATION OF ADVANTAGES TOWARDS EXISTING OBSERVER BASED APPROACHES

Here we use parametric faults of the capacitor as examples to demonstrate the advantages of the proposed method towards existing observer based approaches. In fact, existing observer based approaches can also provide an overall indicator of the health condition of the switching power converter. However, existing approaches are mostly utilized to detect "hard" faults (such as complete failure of a certain element) instead of parametric faults. This is because existing observer based approaches usually utilize a simple threshold of the residuals (or a function of residuals) for fault detection. Without considering the statistic characteristics, these methods have limited sensitivity and therefore sometimes the parametric faults cannot be reliably detected.

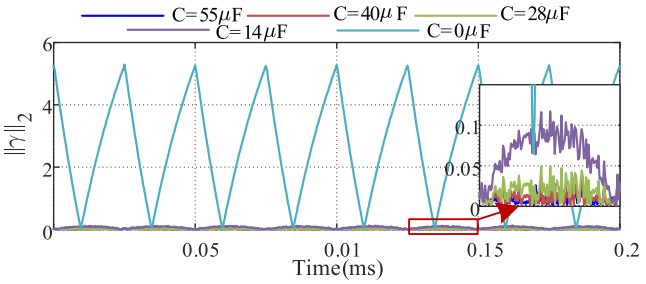

FIGURE 12. Fault detection results of the existing observer based approach in [19] during parametric faults of the capacitor, simulation results.

Next, the performance of the existing observer based approach in [19] is studied to further validate the advantages of the proposed method. The existing method first constructs an observer $\gamma(t)$, and the 2-norm of the observer $||\gamma(t)||_2$ is compared to a pre-defined threshold for the detection of a fault. The results of the existing method with different capacitor parametric faults are shown in Fig. 12. First, one can observe that the value of $||\gamma(t)||_2$ increases significantly when the capacitor is experiencing a complete failure ($C = 0$ μF), which proves that the existing method works well during "hard" faults. However, with parametric faults such as C = 40 μF or 28 μF, the values of $||\gamma(t)||_2$ are on top of each other and in this case a simple threshold may not be sufficient for reliable detection of parametric faults. These results prove the necessity and advantages of the proposed method.

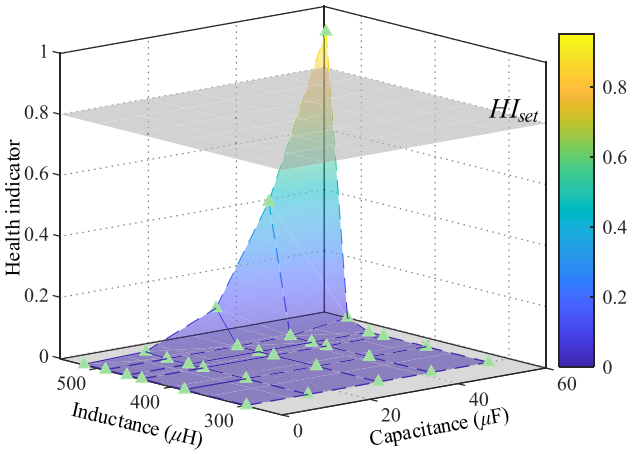

FIGURE 13. Health indicator of the proposed fault detection method during parametric faults of both the inductor and capacitor, simulation results.

D. PARAMETRIC FAULTS OF BOTH THE INDUCTOR AND CAPACITOR

To further validate the effectiveness of the proposed parametric fault detection method, parametric faults with inductor faults and capacitor faults occurring at the same time are further studied. The cases consist of a complete combination of different values of inductances and capacitances in section IV.B and C, resulting in a total number of 30 cases (6 inductances by 5 capacitances). The calculated values of the health indicators are depicted in Fig. 13. The user-defined threshold HI_{set} is also represented in the figure. One can observe that the values of the health indicator are less than HI_{set} for all parametric faults, and are generally lower with more severe parametric faults. Therefore, the proposed method can reliably and sensitively detect parametric faults in all above cases.

V. EXPERIMENTAL RESULTS

The proposed health indicator for parametric fault detection is further validated through hardware experiments. Here the dc-dc buck converter is built with the same topology and setup as in section IV (topology in Fig. 23 of the Appendix and setup in Table 2). The hardware experimental platform is shown in Fig. 14. The available measurements are the same as in section IV and are obtained by the oscilloscope.

To implement parametric faults of inductors and capacitors in the circuit, we replace the inductor and capacitor of the circuit with different combinations of inductor/capacitor units (with units in series or in parallel), as shown in Fig. 15 and Table 3. For the inductors, here 4 inductor units are adopted (with approximate values of 75, 86, 142 and 298 μH, respectively), resulting in 6 different values of inductors (normal operation: 518 μH, parametric faults: 489 μH, 460 μH, 440 μH, 382 μH, and 298 μH). For the capacitors, here 3 capacitor units are adopted, resulting in 3 different values of capacitors (normal operation: 55 μF, parametric faults: 40 μF and 28 μF). The values of the 6 inductors and 3 capacitors

TABLE 3. Parametric fault implementation.

L	518μH	489μH	460μH	440μH	382μH	298μH
Set	(1)+(3)+(4)	(1)//(2)+(3)+(4)	(1)+(2)+(4)	(3)+(4)	(2)+(4)	(4)
C	55μF	40μF	28μF			
Set	(1)	(2)	(3)			

'+' represents the components are connected in series, '//' represents the components are connected in parallel

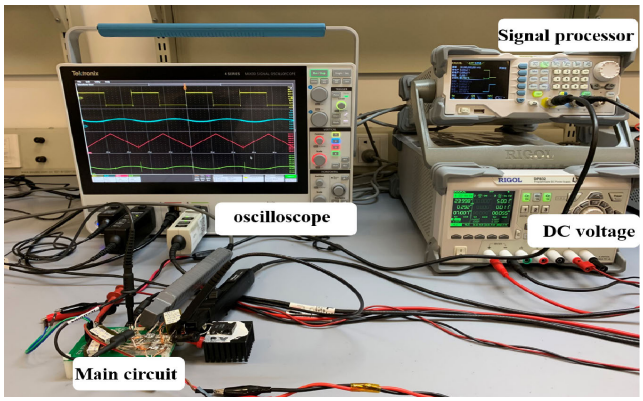

FIGURE 14. Synchronize dc-dc buck converter experiment.

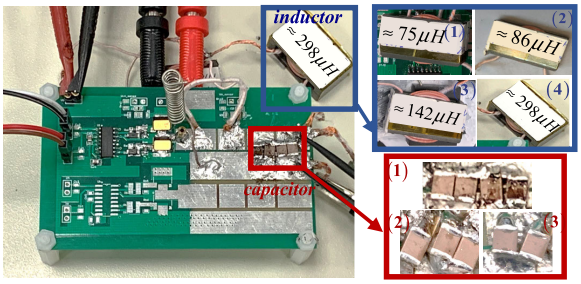

FIGURE 15. Circuit implementation.

are measured offline to ensure the parameter accuracy (one can observe that these values are not exactly the same as the values of corresponding units in series or in parallel, since the values of the inductor/capacitor units are only approximate values). Meanwhile, the other parameters of the circuit remain the same. The user-defined settings are also selected as $\alpha_{set} = 0.5$ and $HI_{set} = 0.8$ empirically.

The screen shot of the oscilloscope during normal operation is shown in Fig. 16. The measurements from the oscilloscope during different inductor parametric faults (1 normal operation + 5 parametric faults) and capacitor parametric faults (1 normal operation + 2 parametric faults) are summarized in Fig. 17 and Fig. 18, respectively (here we re-depict the waveforms of the measurements instead of directly presenting the screen shots of the oscilloscope, to demonstrate the measurement differences among different parametric faults). One can observe that the measurements do not change much with parametric faults.

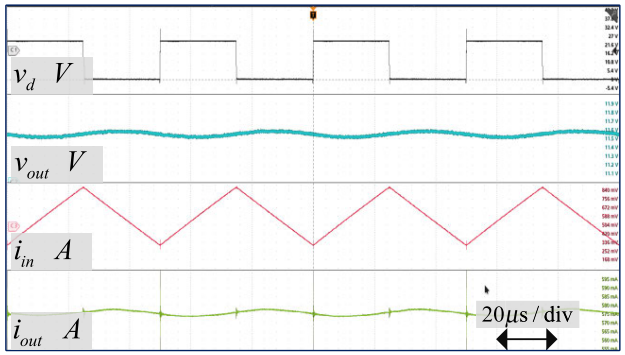

FIGURE 16. Measurements during normal operation, hardware experiments.

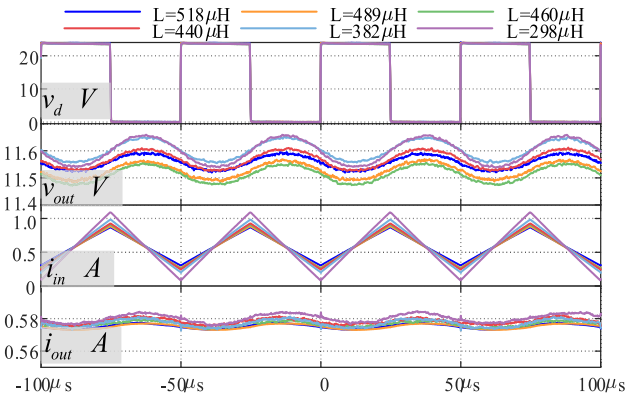

FIGURE 17. Measurements during parametric faults of the inductor, hardware experiments.

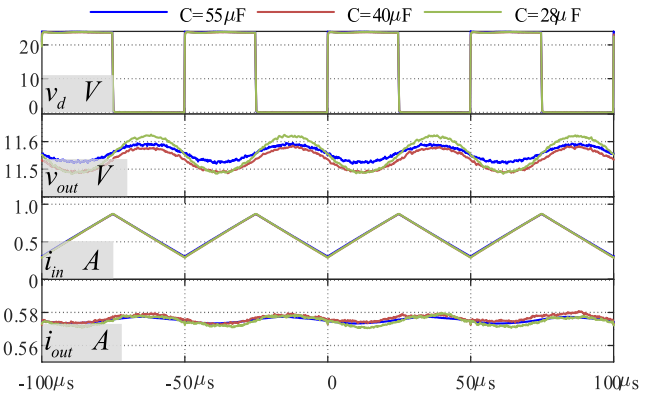

FIGURE 18. Measurements during parametric faults of the capacitor, hardware experiments.

The distribution of the calculated chi-square value during normal operation is depicted in Fig. 19. One can observe that the distribution is close to the ideal distribution. The calculated health indicator is $HI = 0.9140 > HI_{\text{set}}$, implying that the system is healthy. The distributions of the calculated chi-square value during inductor parametric faults and capacitor parametric faults are depicted in Fig. 20 and Fig. 21. It can be observed that the distribution is further away from ideal distribution with more severe parametric faults.

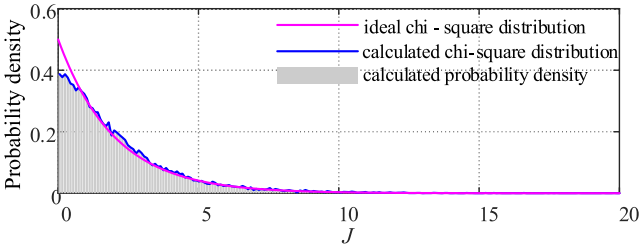

FIGURE 19. Distribution of calculated chi-square value during normal operation, hardware experiments.

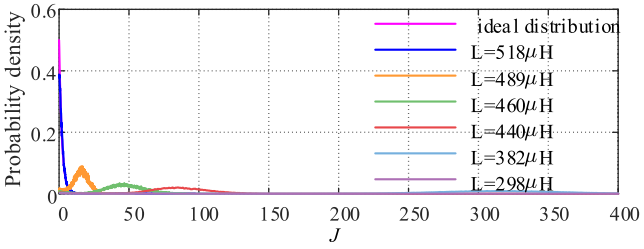

FIGURE 20. Distributions of calculated chi-square value during parametric faults of the inductor, hardware experiments.

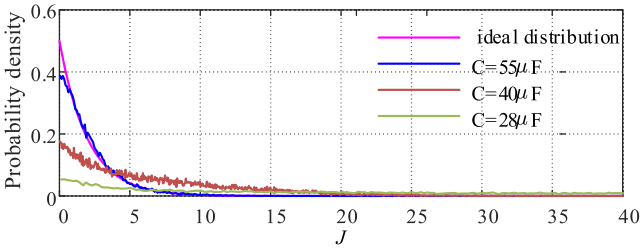

FIGURE 21. Distributions of calculated chi-square value during parametric faults of the capacitor, hardware experiments.

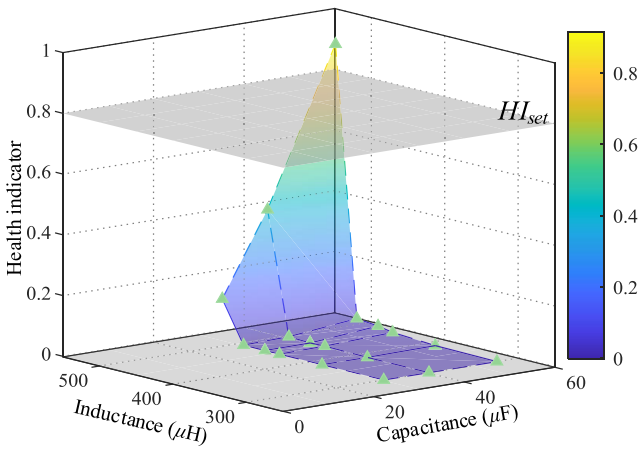

FIGURE 22. Health indicator of the proposed fault detection method during parametric faults of both the inductor and capacitor, hardware experiments.

The calculated health indicators with 489, 460, 440, 382 and 298 μH inductors are $HI = 0.0277$, 0.0203, 0.0113, 0.0025 and 0, respectively. The calculated health indicators with 40 and 28 μF capacitors are $HI = 0.4053$ and 0.1356,

respectively. The parametric faults are successfully detected since $HI < HI_{\text{set}}$ for all above scenarios.

Next, to consider parametric faults cases with inductor faults and capacitor faults occurring at the same time, we further study a complete combination of parametric faults with different values of inductances and capacitances (6 inductances by 3 capacitances, 18 cases in total). The calculated values of the health indicators are depicted in Fig. 22. The user-defined threshold HI_{set} is also represented in the figure. It can be observed that $HI < HI_{\text{set}}$ for all parametric faults, and therefore the parametric faults can be reliably and sensitively detected.

VI. CONCLUSION

This article proposes a model based parametric fault detection method focusing on capacitor and inductor parameter drifts in switching power converters. The parametric fault is detected through a health indicator that represents the overall health condition of the circuit. The method first systematically models the switching power converter in a standard syntax, to accurately consider all the physical laws that the converter circuit should obey during healthy conditions. Next, the states of the system are solved by dynamic state estimation and the health indicator is generated by checking the consistency between the actual measurements and the healthy circuit model. The health indicator utilizes the statistic information of the solution so that the sensitivity of the proposed parametric fault detection method is much improved compared to existing observer based approaches. In addition, since the health indicator can reflect any parametric fault in the switching power converter, estimating all the parameters of the circuit at the same time is not required compared to existing parameter identification based approaches. Simulation and experimental results in an example buck converter demonstrate the effectiveness of the proposed parametric fault detection method.

TABLE 4. Possible values of switch status vector in CCM.

Operating Mode	*1*	*2*
$\boldsymbol{S}(t)$	$[1,0]^T$	$[0,1]^T$

APPENDIX

This Appendix demonstrates the detailed mathematical model of an example dc-dc buck converter, as shown in Fig. 23. The inductor is modeled as the inductance L in series with the inductance body resistance R_L. The capacitor is modeled as the capacitance C in series with the equivalent series resistance (ESR) R_C. The resistive load is modeled as the resistance R. The status of the two switches can be represented in the switch status vector $\boldsymbol{S}(t) = [S_1(t), S_2(t)]^T$, where $S_1(t)$ and $S_2(t)$ correspond to the binary status of the switch SW1 and SW2, respectively. The possible values of $\boldsymbol{S}(t)$ in continuous conduction mode (CCM) are shown in Table 4.

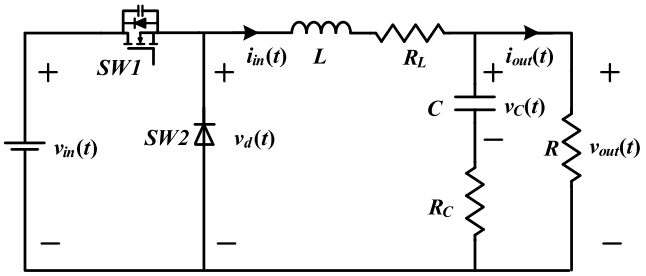

FIGURE 23. dc-dc buck converter equivalent circuit.

The actual measurements of the switching power converter can be selected as the voltages and currents at terminals of the converter. Specifically, the measurements of the buck converter include input voltage $v_{in}(t)$, input current $i_{in}(t)$, output voltage $v_{out}(t)$ and output current $i_{out}(t)$. Note that for this buck converter, the modeling complexity can be further reduced if the measurement $v_{in}(t)$ is substituted by $v_d(t)$. In this case the voltage across SW2 can be directed measured instead of being represented by $v_{in}(t)$ and $\boldsymbol{S}(t)$. In this case, the mathematical model of the switching power converter is the same for the two operating modes. With the syntax in (2), the matrices are,

$$\boldsymbol{z}_{actual}(t) = [\, v_d(t)\ v_{out}(t)\,]^T, \boldsymbol{y}_{actual}(t) = [\, i_{in}(t)\ i_{out}(t)\,]^T,$$
$$\boldsymbol{x}(t) = [\, v_C(t)\ i_{in}(t)\ i_{out}(t)\,]^T, \boldsymbol{A}_{eq1} = \begin{bmatrix} 1 & R_L + R_C & -R_C \\ 1 & R_C & -R_C \end{bmatrix},$$
$$\boldsymbol{B}_{eq1} = \begin{bmatrix} 0 & L & 0 \\ 0 & 0 & 0 \end{bmatrix}, \boldsymbol{A}_{eq2} = \begin{bmatrix} 0 & -1 & 1 \end{bmatrix}, \boldsymbol{B}_{eq2} = \begin{bmatrix} C & 0 & 0 \end{bmatrix},$$
$$\boldsymbol{A}_{eq3} = \begin{bmatrix} 0 & 1 & 0 \\ 0 & 0 & 1 \end{bmatrix} \text{ and the remaining matrices are null or 0.}$$

REFERENCES

[1] M. Shahbazi, E. Jamshidpour, P. Poure, S. Saadate, and M. R. Zolghadri, "Open- and short-circuit switch fault diagnosis for nonisolated DC–DC converters using field programmable gate array," *IEEE Trans. Ind. Electron.*, vol. 60, no. 9, pp. 4136–4146, Sep. 2013.

[2] S. Yang, D. Xiang, A. Bryant, P. Mawby, L. Ran, and P. Tavner, "Condition monitoring for device reliability in power electronic converters: A review," *IEEE Trans. Power Electron.*, vol. 25, no. 11, pp. 2734–2752, Nov. 2010.

[3] Z. Gao, C. Cecati, and S. X. Ding, "A survey of fault diagnosis and fault-tolerant techniques—Part I: Fault diagnosis with model-based and signal-based approaches," *IEEE Trans. Ind. Electron.*, vol. 62, no. 6, pp. 3757–3767, Jun. 2015.

[4] Z. Gao, C. Cecati, and S. X. Ding, "A survey of fault diagnosis and fault-tolerant Techniques—Part II: Fault diagnosis with knowledge-based and Hybrid/Active approaches," *IEEE Trans. Ind. Electron.*, vol. 62, no. 6, pp. 3768–3774, Jun. 2015.

[5] J. O. Estima and A. J. Marques Cardoso, "A new algorithm for real-time multiple open-circuit fault diagnosis in voltage-fed PWM motor drives by the reference current errors," *IEEE Trans. Ind. Electron.*, vol. 60, no. 8, pp. 3496–3505, Aug. 2013.

[6] S. Nie, X. Pei, Y. Chen, and Y. Kang, "Fault diagnosis of PWM DC–DC converters based on magnetic component voltages equation," *IEEE Trans. Power Electron.*, vol. 29, no. 9, pp. 4978–4988, Sep. 2014.

[7] M. Bhardwaj, S. Choudhury, R. Poley, and B. Akin, "Online frequency response analysis: A powerful plug-in tool for compensation design and health assessment of digitally controlled power converters," *IEEE Trans. Ind. Appl.*, vol. 52, no. 3, pp. 2426–2435, May/Jun. 2016.

[8] J.-K. Park and J. Hur, "Detection of inter-turn and dynamic eccentricity faults using stator current frequency pattern in IPM-type BLDC motors," *IEEE Trans. Ind. Electron.*, vol. 63, no. 3, pp. 1771–1780, Mar. 2016.

[9] A. Bouzida, O. Touhami, R. Ibtiouen, A. Belouchrani, M. Fadel, and A. Rezzoug, "Fault diagnosis in industrial induction machines through discrete wavelet transform," *IEEE Trans. Ind. Electron.*, vol. 58, no. 9, pp. 4385–4395, Sep. 2011.

[10] M. M. Rahman and M. N. Uddin, "Online unbalanced rotor fault detection of an IM drive based on both time and frequency domain analyses," *IEEE Trans. Ind. Appl.*, vol. 53, no. 4, pp. 4087–4096, Jul. 2017.
[11] Y. Trachi, E. Elbouchikhi, V. Choqueuse, and M. E. H. Benbouzid, "Induction machines fault detection based on subspace spectral estimation," *IEEE Trans. Ind. Electron.*, vol. 63, no. 9, pp. 5641–5651, Sep. 2016.
[12] S. Yin, S. X. Ding, X. Xie, and H. Luo, "A review on basic data-driven approaches for industrial process monitoring," *IEEE Trans. Ind. Electron.*, vol. 61, no. 11, pp. 6418–6428, Nov. 2014.
[13] Z. Gao, S. X. Ding, and C. Cecati, "Real-time fault diagnosis and fault-tolerant control," *IEEE Trans. Ind. Electron.*, vol. 62, no. 6, pp. 3752–3756, Jun. 2015.
[14] S. Mohagheghi, R. G. Harley, T. G. Habetler, and D. Divan, "Condition monitoring of power electronic circuits using artificial neural networks," *IEEE Trans. Power Electron.*, vol. 24, no. 10, pp. 2363–2367, Oct. 2009.
[15] W. Chen and A. M. Bazzi, "Logic-based methods for intelligent fault diagnosis and recovery in power electronics," *IEEE Trans. Power Electron.*, vol. 32, no. 7, pp. 5573–5589, Jul. 2017.
[16] L. Wen, X. Li, L. Gao, and Y. Zhang, "A new convolutional neural network-based data-driven fault diagnosis method," *IEEE Trans. Ind. Electron.*, vol. 65, no. 7, pp. 5990–5998, Jul. 2018.
[17] Q. Lin, S. Chen, and C.-M. Lin, "Parametric fault diagnosis based on fuzzy cerebellar model neural networks," *IEEE Trans. Ind. Electron.*, vol. 66, no. 10, pp. 8104–8115, Oct. 2019.
[18] B. Cai, Y. Zhao, H. Liu, and M. Xie, "A data-driven fault diagnosis methodology in three-phase inverters for PMSM drive systems," *IEEE Trans. Power Electron.*, vol. 32, no. 7, pp. 5590–5600, Jul. 2017.
[19] J. Poon, P. Jain, I. C. Konstantakopoulos, C. Spanos, S. K. Panda, and S. R. Sanders, "Model-based fault detection and identification for switching power converters," *IEEE Trans. Power Electron.*, vol. 32, no. 2, pp. 1419–1430, Feb. 2017.
[20] N. Wassinger, E. Penovi, R. G. Retegui, and S. Maestri, "Open-circuit fault identification method for interleaved converters based on time-domain analysis of the state observer residual," *IEEE Trans. Power Electron.*, vol. 34, no. 4, pp. 3740–3749, Apr. 2019.
[21] S. Shao, P. W. Wheeler, J. C. Clare, and A. J. Watson, "Fault detection for modular multilevel converters based on sliding mode observer," *IEEE Trans. Power Electron.*, vol. 28, no. 11, pp. 4867–4872, Nov. 2013.
[22] M. Al-Greer, M. Armstrong, M. Ahmeid, and D. Giaouris, "Advances on system identification techniques for DC–DC switch mode power converter applications," *IEEE Trans. Power Electron.*, vol. 34, no. 7, pp. 6973–6990, Jul. 2019.
[23] K. Yao, W. Tang, W. Hu, and J. Lyu, "A current-sensorless online ESR and C identification method for output capacitor of buck converter," *IEEE Trans. Power Electron.*, vol. 30, no. 12, pp. 6993–7005, Dec. 2015.
[24] J. Poon, P. Jain, C. Spanos, S. K. Panda, and S. R. Sanders, "Fault prognosis for power electronics systems using adaptive parameter identification," *IEEE Trans. Ind. Appl.*, vol. 53, no. 3, pp. 2862–2870, May 2017.
[25] M. Ahmeid, M. Armstrong, S. Gadoue, M. Al-greer, and P. Missailidis, "Real-time parameter estimation of DC–DC converters using a self-tuned Kalman filter," *IEEE Trans. Power Electron.*, vol. 32, no. 7, pp. 5666–5674, Jul. 2017.
[26] M. A. Vogelsberger, T. Wiesinger, and H. Ertl, "Life-cycle monitoring and voltage-managing unit for DC-link electrolytic capacitors in PWM converters," *IEEE Trans. Power Electron.*, vol. 26, no. 2, pp. 493–503, Feb. 2011.
[27] Y. Liu, A. P. S. Meliopoulos, R. Fan, L. Sun, and Z. Tan, "Dynamic state estimation based protection on series compensated transmission lines," *IEEE Trans. Power Del.*, vol. 32, no. 5, pp. 2199–2209, Oct. 2017.

KANG YUE (Student Member, IEEE) received the B.S. degree in electrical engineering and its automation from the Hefei University of Technology, Hefei, China, in 2017. She is currently pursuing the Ph.D. degree with the Power System Protection and Automation Laboratory, School of Information Science and Technology, ShanghaiTech University. Her research interests include health monitoring and the parameter identification of power electronic systems.

YU LIU (Member, IEEE) received the B.S. and M.S. degrees in electrical power engineering from Shanghai Jiao Tong University, Shanghai, China, in 2011 and 2013, respectively, and the Ph.D. degree in electrical and computer engineering from the Georgia Institute of Technology, Atlanta, GA, USA, in 2017. He is currently a tenure-track Assistant Professor with the School of Information Science and Technology, ShanghaiTech University, Shanghai. His research interests include modeling, protection, fault location, the state/parameter estimation of power systems, and power electronic systems.

PENG ZHAO (Graduate Student Member, IEEE) received the B.S. degree in electrical engineering from the Hefei University of Technology, Hefei, China, in 2017. He is currently pursuing the Ph.D. degree in power electronics with the School of Information Science and Technology, ShanghaiTech University, Shanghai, China.

His current research interests include the small and medium power application of inductive power transfer systems, and resonant converters.

BINGLIN WANG (Student Member, IEEE) received the B.S. degree in electrical engineering and intelligent control from the Xi'an University of Technology, Xi'an, Shaanxi, China, in 2018. He is currently pursuing the Ph.D. degree in electrical engineering with the School of Information Science and Technology, ShanghaiTech University, Shanghai, China. His research interests include protection, fault location, and state estimation.

MINFAN FU (Senior Member, IEEE) received the B.S., M.S., and Ph.D. degrees in electrical and computer engineering from the University of Michigan-Shanghai Jiao Tong University Joint Institute, Shanghai Jiao Tong University, Shanghai, China, in 2010, 2013, and 2016, respectively.

From 2016 to 2018, he held a postdoctoral position with the Center for Power Electronics Systems, Virginia Polytechnic Institute and State University, Blacksburg, VA, USA. He is currently an Assistant Professor with the School of Information Science and Technology, ShanghaiTech University, Shanghai. His research interests include megahertz wireless power transfer, high frequency power conversion, high-frequency magnetic design, and the application of wide-bandgap devices.

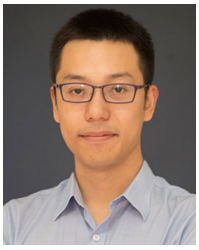

HAOYU WANG (Senior Member, IEEE) received the bachelor's degree (Hons.) from Zhejiang University, Hangzhou, China, and the master's and Ph.D. degrees in electrical engineering from the University of Maryland at College Park, College Park, MD, USA.

He is currently a Tenured Associated Professor with the School of Information Science and Technology, ShanghaiTech University, Shanghai, China. His research interests include power electronics, plug-in electric and hybrid electric vehicles, the applications of wide-bandgap semiconductors, renewable energy harvesting, and power management integrated circuits.

Dr. Wang is an Associate Editor of the IEEE TRANSACTIONS ON INDUSTRIAL ELECTRONICS and the IEEE TRANSACTIONS ON TRANSPORTATION ELECTRIFICATION, and a Guest Associate Editor of the *CPSS Transactions on Power Electronics and Applications*.